Nano Energy 105 (2023) 108027

Contents lists available at ScienceDirect

Nano Energy

journal homepage: www.elsevier.com/locate/nanoen

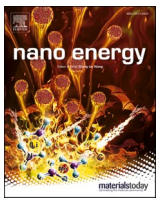

High-entropy alloy catalysts: Fundamental aspects, promises towards electrochemical NH_3 production, and lessons to learn from deep neural networks

Rafael B. Araujo *, Ilknur Bayrak Pehlivan, Tomas Edvinsson *

Department of Materials Science and Engineering, Solid State Physics, Uppsala University, Box 35, 75103 Uppsala, Sweden

ARTICLE INFO

Keywords:
High-entropy alloys
Electrocatalytic nitrogen reduction
Scaling-relations
Machine learning
Deep neural networks

ABSTRACT

A computational approach to judiciously predict high-entropy alloys (HEAs) as an efficient and sustainable material class for the electrochemical reduction of nitrogen is here presented. The approach employs density functional theory (DFT), adsorption energies of N atoms and N_2 molecules as descriptors of the catalytic activity and deep neural networks. A probabilistic approach to quantifying the activity of HEA catalysts for nitrogen reduction reaction (NRR) is described, where catalyst elements and concentration are optimized to increase the probability of specific atomic arrangements on the surfaces. The approach provides key features for the effective filtering of HEA candidates without the need for time-consuming calculations. The relationships between activity and selectivity, which correlate with the averaged valence electron concentration and averaged electronegativity of the reference HEA catalyst, are analyzed in terms of sufficient interaction for sustained reactions and, at the same time, for the release of the active site. As a result, a complete list of 3000 HEAs consisting of quinary components of the elements Mo, Cr, Mn, Fe, Co, Ni, Cu, and Zn are reported together with their metrics to rank them from the most likely to the least likely active catalysts for NRR in gas diffusion electrodes, or for the case where non-aqueous electrolytes are utilized to suppress the competing hydrogen evolution reaction. Moreover, the energetic landscape of the electrochemical NRR transformations are computed and compared to the case of Fe. The study also analyses and discusses how the results would translate to liquid-solid reactions in aqueous electrochemical cells, further affected by changes in properties upon hydroxylation, oxygen, hydrogen, and water coverages.

1. Introduction

Supplying most of the energy consumed by our society from fossil fuels is at risk of critically affecting global warming due to net CO_2 emissions into the atmosphere [1]. An energy matrix transformation from the currently used net emission sources to CO_2 neutrality is essential to achieve energy sustainability. An increased production of energy from renewable energy sources such as wind-, solar-, hydro-, or geopower would here be highly desired. However, several of these energy resources are highly intermittent, geographically spread, or seasonally dependent. Achieving an efficient and large-scale compatible way of storing the produced energy would be highly beneficial. In this context, ammonia emerges as a promising candidate both as a fertilizing chemical and as a potential energy vector that benefits from its high hydrogen content and easy liquefaction. Currently, ammonia is industrially produced via the Haber-Bosch process, which demands a large amount of energy and releases CO_2 into the atmosphere, thus aggravating the greenhouse effect. One strategy to circumvent this is to produce ammonia in an eco-friendly process, which could be an electrochemical synthesis of ammonia from nitrogen gas using sustainably produced electricity. A severe bottleneck of electrochemical ammonia synthesis, is the low ammonia production rates of about microgram per hour per square centimeter-level, often lower than 10% Faradaic efficiencies (FEs), and stability issues. Therefore, the development of suitable materials plays an important role in mitigating such issues and achieving industrial application [2]. In this context, high-entropy alloys (HEAs) emerge as a new class of catalysts that provide unprecedented compositional diversity that hold the promise to tune reaction pathways and, thus, selectivity and rates, alongside entropic stabilization of the material.

* Corresponding authors.
E-mail addresses: rafael.araujo@angstrom.uu.se (R.B. Araujo), tomas.edvinsson@angstrom.uu.se (T. Edvinsson).

https://doi.org/10.1016/j.nanoen.2022.108027
Received 28 October 2022; Accepted 18 November 2022
Available online 19 November 2022

The concept of multi-component alloys with entropy stabilization came out around 2004 when two independent research groups showed that multiple-element materials containing at least five different species could be formed into a homogeneous phase [3,4]. The thermodynamically and kinetically stabilized structures of HEAs provide high fracture resistance, ductility, and physicochemical stability, thus enabling employment in harsh environments [5–7]. Concerning their application in catalysis, these alloys form a promising new material class and is a rapidly growing research field [5,6]. As an advantage, the multi-component form of HEAs can provide several active sites on a catalytic surface and structural stability. The complexity of the catalytic surface enables the possibility of breaking the symmetry rules imposed by the scaling relationships [8], which in principle opens the possibility of finding highly active catalysts for different reactions.

It is notoriously challenging to reduce nitrogen to form ammonia electrochemically due to the scaling relationships and simultaneous ability to reduce hydrogen in a protonic system, and thus a competition between the nitrogen reduction reaction (NRR) and the hydrogen evolution reaction (HER). Although N_2 is the most abundant molecule in the atmosphere, its triple bond and the lack of dipole moments make it a highly inert specie and, hence, very hard to catalyze due to the lack of nitrogen fixation on catalytic surfaces [9]. Several strategies have been reported in the literature to enhance NRR, where they all more or less are related to nitrogen fixating surfaces with either proton deficiency or electron starving (and thus low rate) [9–14]. Especially interesting for this work are the results reported by D. Zhang et al. [15]. They were one of the first groups reporting that HEAs could be used to reduce nitrogen, where 38.5% FE was achieved using HEA RuFeCoNiCu nanoparticles with a small size of 16 nm and signifies the promises of the approach, although the remaining challenge is to perform the reaction with NRR selectivity versus HER also at high rates.

The present work focuses on two important aspects of the application of HEAs to NRR: *i)* a rational strategy to screen over an ample search space of quinary HEAs formed with Mo-Cr-Mn-Fe-Co-Ni-Cu-Zn working as novel catalysts for NRR, without the inclusion of Ru or other platinium group metals (PGMs), and *ii)* identifying relationships between HEAs intrinsic properties and their catalytic activity. The search for alternative catalysts for NRR in the wide range of compositional space found in the quinary HEAs is performed by employing the framework of the density functional theory (DFT), machine learning techniques and a probabilistic approach developed by T. A. Batchelor et al. [16]. Similar strategies were also applied, successfully, by T. A. Batchelor et al. [16], J. K. Pedersen et al. [17] and W. A. Saidi et al. [18]. They used DFT to train machines over hundreds of adsorption energies on HEAs microstates and, further, used these machines to screen for selective and active catalysts for oxygen, carbon dioxide, carbon monoxide reduction reactions and also ammonia oxidation, respectively. The estimated catalytic activities are, further correlated with intrinsic properties of the HEAs, like the average valence electron concentration and their electronegativity. This might help to understand the main properties that dictate the electrochemical transformations and it is also a simplified path to selecting promising catalysts. Finally, since a clear reaction pathway on the surface of a HEA is not possible due to their inherent randomness, a statistical analysis of the reaction pathway will be performed for the selected HEAs.

The associative pathways (distal/alternating and enzymatic) are the most favorable ones when electrochemical NRR is in focus [19]. This is due to the high activation barriers to dissociating N_2* into 2 N*, that, for instance, is of the order of 1.77 eV for the case of Ru(0001) [20]. The other two likely options are the distal/alternating pathways and the enzymatic pathway [21]. Pedersen et al. [22] recently showed that species on threefold hollow sites of HEAs could partially circumvent scaling relations with the adsorption of species on top sites due to the different coordination of threefold sites compared to on top sites (also confirmed in this work). Moreover, Singh et al. [19] and Montoya et al. [23] showed that the two potential limiting steps of the NRR reaction on transition metal surfaces are the hydrogenation of N_2* forming NNH* and the desorption of NH* forming NH_2 * . In the distal pathway, the N_2* adsorbs on the top position while the NH* adsorbs on the threefold hollow site. Hence, the scaling relationship between these two steps can be circumvented due to the randomness of the HEA surfaces. That allows us to seek highly active HEAs for NRR that deliver strong N_2 * bond interaction in the distal position (adsorbing on the top site), but still with lower desorption of the NH* intermediate. Therefore, we will focus on identifying HEAs that optimize the catalytic activity and selectivity towards NRR following the distal/alternating pathway. Moreover, only for the selected catalysts, we explicitly compute, with the DFT framework, the potential limiting steps, $N_{2(gas)}+*\rightarrow N_2*$, $N_2*+H^+ + e^- \rightarrow NNH*$ and $NH*+H^+ + e^- \rightarrow NH_2*$ for 100 microstates of the referent HEA and show how the reaction pathways can be depicted based on the statistical analysis.

Tuning to the approach to characterize the reaction steps, Singh et al. [19] and Montoya et al. [23] have shown that the N* is a descriptor of the NRR catalytic activity on transitions metals where, for the case of close-packed structures, Fe is placed on the top of the volcano curve [19]. Therefore, we can employ this descriptor to optimize HEAs elemental concentrations that maximize the local sites with similar adsorption energies as in the case of Fe, for instance. That must lead to optimal cases with reasonable potential limiting steps – at least similar to the value displayed by Fe. Moreover, it allows us to build a much more efficient screening strategy since the number of parameters is reduced. That in itself should be enough to deliver promising HEA catalysts for NRR. However, due to the break of scaling relationships, the top of the volcano curve is not completely known and, hence, including the N_2* also in the optimization process might lead to cases with even higher activity and that can also mitigate the N_2 fixation issue. It is also important to highlight that the activations barrier of the NRR following the distal pathway tends to be very similar to the computed thermodynamical barriers. E. Tayyebi et al. [20] and A. B. Höskuldsson et al. [24] have shown that including activation barriers in the calculation of N_2 reduction pathways leads to the same electrochemical paths predicted with thermochemistry, for Ru(0001) and W(110). Moreover, the transition states computed for small molecules like N_2, are often resembling the final state of the reaction [25]. Therefore, confirming that thermodynamical steps, in this case, can be used as an effective parameter to estimate the rates of the reaction.

2. Method

The approach to model the reactions and to screen over the HEA's elemental concentration pool is depicted in Fig. 1 and based on the following steps:

1. Quinary HEAs formed with the elements Mo-Cr-Mn-Fe-Co-Ni-Cu-Zn are randomly created. DFT calculations are performed over 1200 microstructures formed with the above-mentioned elements. For each microstructure, the adsorption energies of N_2 * and N * (descriptors of the reaction) are computed and stored in a database (DFT details are in the section "***DFT Calculations***").
2. Representation models of the microstructures are created and used to build neural network models that are trained on the adsorption energies from the DFT calculations. These models can compute adsorption energies almost instantaneously and, overcome the time-consuming task of performing thousands of adsorption energies with the DFT approach (details are in the section "***Deep neural networks***").
3. Using the deep neural network models, we calculate the adsorption energy of N * and N_2 * (descriptors of the catalytic activity) on 2000 microstates of each of the 3000 HEAs considered here (an impossible job if DFT would be directly employed). The constraint that species concentration must be lower than 50% is used. A higher concentration of a specific species reduces the entropic effects that stabilize

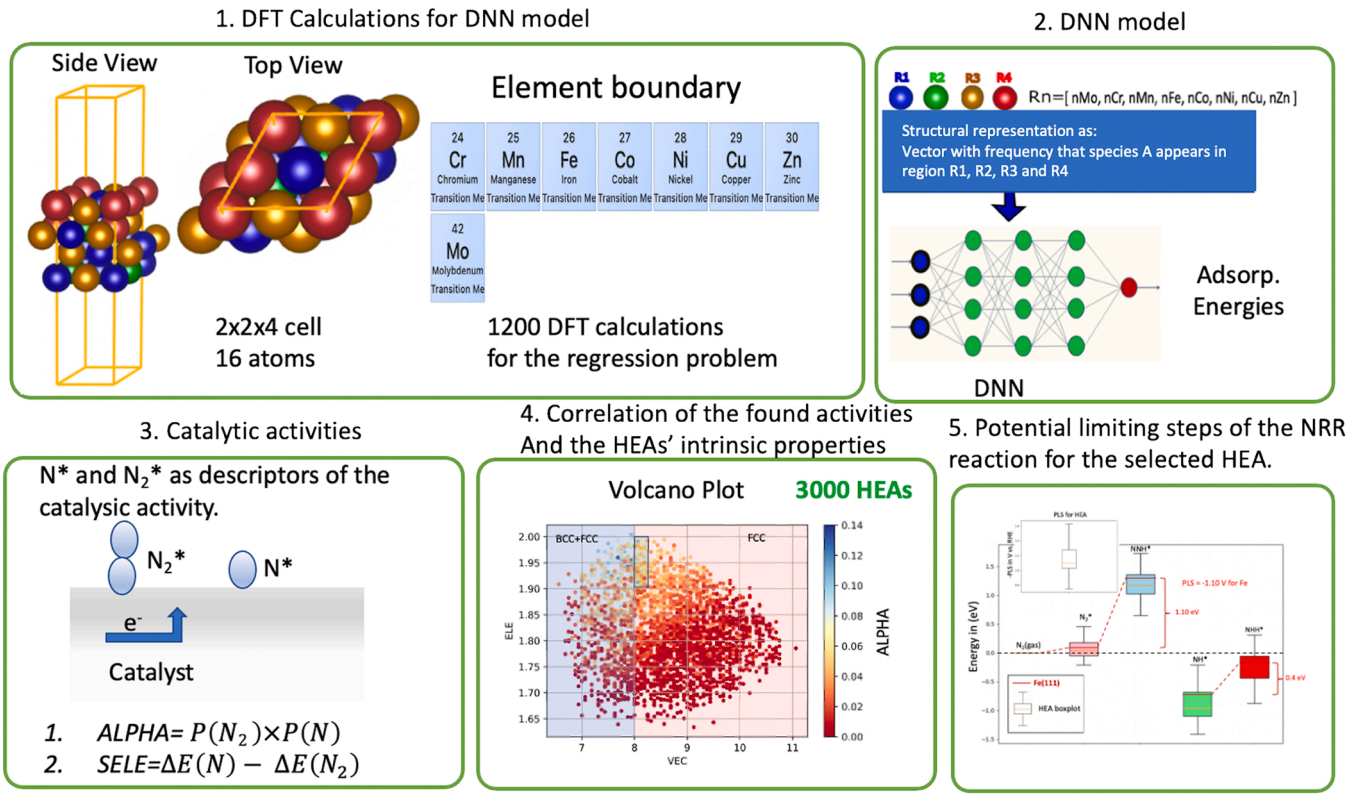

Fig. 1. Schematic picture of the main steps employed here to select optimum catalysts for NRR.

these catalysts. Hence, increasing the probability of structural dissociation into multiple phases, for instance. The probabilistic approach is, hence, used together with the adsorption energies to estimate catalytic activities (as described in the section "***Towards active HEAs for NRR***") and also selectivities (as described in the section "***Towards Selectivity***").

4. Inherent properties of the HEAs like the averaged valence electron concentration (VEC), averaged electronegativity (ELE) and averaged working function (WF) are correlated with the estimated activities to unravel the properties controlling the activity and selectivity.
5. The thermodynamical barriers of the potential limiting steps are calculated for 100 microstructures of a selected HEA. These are shown in the form of box plots and compared with the case of Fe (111) (details are in the section "***Potential limiting steps of the selected HEA***").

DFT calculations: The projected augmented wave method was used to solve the Kohn-Sham equations implemented in the Vienna ab initio Simulation Package (VASP) [26,27]. The wave functions were expanded using plane waves with a cutoff energy of 400 eV while a (4×4×1) *k*-point mesh was used to sample over the Brillouin zone. Smearing of 0.2 eV was employed to obtain partial occupations using the Methfessel-Paxton scheme of second order. Spin-polarized orbitals were used in the ferromagnetic (FM) state and the Bayesian error estimation functional with van der Waals correlation (BEEF-vdW) [28] was utilized to describe the Kohn-Sham Hamiltonian's exchange and correlation term. The BEEF-vdW has been reported to be one of the most accurate functionals to describe adsorption energies on transition metal surfaces [29,30], and is the approach chosen for this study. The structural models were built into a 2×2×4 face-centered cubic (FCC) (111) slab with a vacuum of 20 Å to avoid interaction amongst periodic images, allowing the two topmost layers to geometrically relax. In contrast, the two bottom layers were fixed to the optimized bulk structure. Atoms positions were optimized until a maximum force of 0.08 eV/Å was obtained. It is common for calculation where single atoms are used forces convergence of the order of 0.03–0.01 eV/Å. However, the randomness of the HEAs adds complexity and lower convergence parameters need to be used. Other references have also employed this value [16,17]. Moreover, we tested for one case of N * with force convergence of 0.03 eV/Å. We got a difference of 0.02 eV in the adsorption energy. Lattice parameters of the slabs were set on a weighted average basis and assuming species has FCC bulk structures, similar to the work of T. A. Batchelor et al. [16]. Moreover, Clausen et al. [31] showed that possible remaining strain effects on the adsorption energy of small molecules are alleviated by the inherent distortion of the lattice in HEAs. Bulk optimizations were performed with a *k*-point mesh of 15×15×15 in an FCC structure, and the obtained lattice parameters are summarized in Table S1.

Deep neural network: Although the values of ALPHA could be estimated under any first-principle approach, the high amount of possible microstructures makes the calculation of the N and N_2 adsorption energies non-feasible from a computational time point of view. To circumvent this issue, a representation model of the microstructures that enables establishing a deep neural network (DNN) model permitting the computation of N and N_2 adsorption energies almost instantaneously was built and used together with the DFT calculations. Though the DFT calculations were performed on 1200 microstructures, after data cleaning, the DNN was trained using 784 adsorption energies for N atoms sited on the hexagonal-close-packed sites. We have shown that N adsorbs strongly on this site (see Fig. S2), which also corroborates with the results of W. A. Saidi et al. [18]. For the case of N_2, 784 adsorption energies of the N_2 molecule on randomly created slabs were used to train the DNN model. The representation used to feed the DNN involves the specification of four regions of the HEAs microstructures and frequency counting of species on each specific region (Fig. 2). These regions are then concatenated into a vector defining a regression problem, $\Delta E_{N,N2} = \sum_p^R \sum_k^{metals} C_{p,k} N_{p,k}^i$, where $N_{p,k}^i$ is the number of atoms of specie k in the region p and R is the total number of regions, solved with the DNN. Each

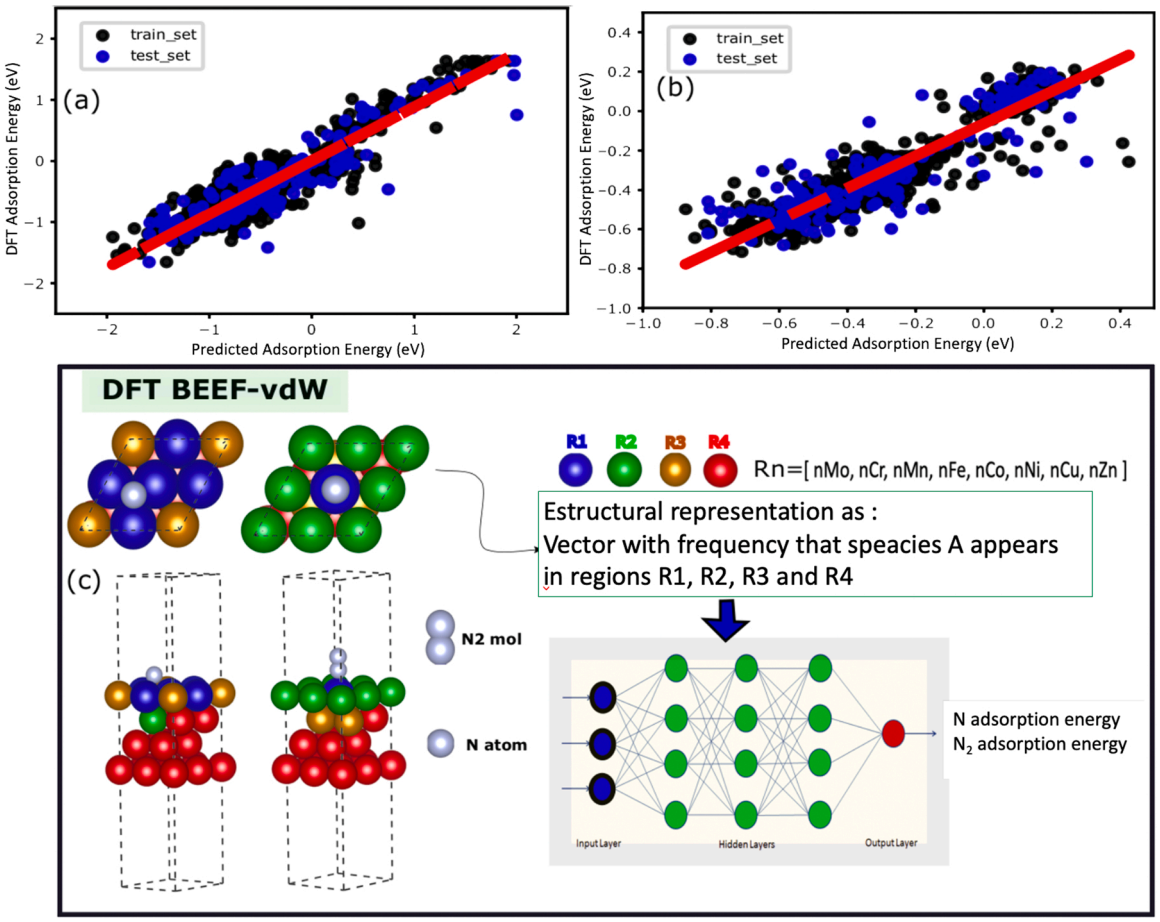

Fig. 2. Comparison between the predicted adsorption energies with the DNN and the computed energies of (a) N and (b) N_2 adsorptions. Blue is the data used in the test set, while black dots are the data of the train set. (c) schematic illustration of the representation used to convert an atomic structure into a numerical vector to feed the DNN and assess activities and selectivities. The structural representation lies in counting species frequencies in specified regions of the unit cell.

built vector represents one microstructure of a HEA of a specific concentration.

The DNNs were built using the Keras library [32]. The data was trained in several networks where the best models were composed of dense sequential layers. The input layers were set with two hundred neurons and a linear activation function for the N adsorption energy and one hundred neurons together with a linear activation function for the dinitrogen adsorption energy. Six hidden layers composed of two hundred neurons each and a "relu" activation function were employed for the N adsorption training, while for the N_2 adsorption training, one layer with 50 neurons and a "relu" activation function (L2 regularization function were employed in both cases). The output layers were built with a linear function. Loss function (mean squared error, MSE) between predicted adsorption energies and DFT computed adsorption energies were minimized using an Adam optimizer with a learning rate of 0.014. Our dataset utilized to build the DNN was randomly divided into a training set (80%) and test set (20%) for both N and N_2 adsorption energies. The evolution of the loss function with the epoch number (training steps) is shown in Fig. S4 and confirms no overfitting phenomena.

Towards active HEAs for NRR: A probabilistic approach based on the adsorption of N_2 molecules and N atoms on the HEAs surface is employed to estimate the catalytic activity of HEAs. The basic principles of the approach were firstly proposed by T. A. Batchelor et al. [16] and are here further expounded on and extended to the use in NRR. The first assumption is that bonds formed between small molecules and catalytic surfaces have a local character, hence, are determined by the microstructure of the local site. This means that the vast composition of the HEA can be approached as an average over microstructures of the HEA, where each microstructure will contribute to the activity in a specific way, depending on the adsorption energy of N in the respective site. This is an approximation that concurs with the experimental situation with a random mixing and atomic dispersion in a real HEA. Moreover, the N_2 fixation issue is accounted for by introducing the N_2 adsorptions energy in the model. In a technical sense, to maximize the number of randomly created sites that deliver: i) Adsorption energies of N in between the obtained values for Fe and Ru. Ru has been proven to show activity towards NRR [33–35], while Fe is a known to be an efficient electrocatalyst for ammonia production [36,37] and appears at the top of the volcano plot – lower limit potential step [19]. Therefore, maximizing microstructures with similar N adsorption energy should ensure high catalytic activity for the specific HEA towards NRR. ii) To identify the number of sites that adsorbs N_2 exothermically – better N_2 fixation. These assumptions can be formulated into a probabilistic approach with:

$$P(N_2) = \frac{\sum Microstructures \quad with \quad \Delta E_{N_2} < -0.5eV}{\sum All \quad considered \quad Microstructures} \tag{1}$$

$$P(N) = \frac{\sum Microstructures \quad with \Delta E_N(\mathrm{Fe}) < \Delta E_N < \Delta E_N(\mathrm{Ru})}{\sum All \quad considered \quad Microstructures} \tag{2}$$

$$\mathrm{ALPHA} = \mathrm{P}(\mathrm{N}_2) \times \mathrm{P}(\mathrm{N}) \tag{3}$$

where $P(N_2)$ is the probability of finding sites with exothermic adsorption for N_2, $P(N)$ is the probability of finding microstructures with energy between ΔE_N(Fe) and ΔE_N(Ru) ALPHA is the probability of the two events happening. A HEA with high ALPHA should thus deliver high

activity, while each microstructure is randomly created with the constraint that its species concentration reassembles a specific HEA concentration.

The Gibbs free energy variation of the reaction $N_2 + * \rightarrow N_2*$ can be calculated as $\Delta G = \Delta E + \Delta ZPE + (\Delta H_{vib} + \Delta H_{rot} + \Delta H_{trans}) - T(\Delta S_{vib} + \Delta S_{rot} + \Delta S_{trans})$ where ΔZPE is the variation on the zero-point energy, ΔH and ΔS are the variations of enthalpy and entropy, respectively, and ΔE is the electronic energy change. To further validate and assess the parameters, we have suggested that a complete vibrational frequencies calculation is performed using DFT to assess the thermal effects. Performing this for conformations in the set, we find that

$$\Delta ZPE + (\Delta H_{vib} + \Delta H_{rot} + \Delta H_{trans}) - T(\Delta S_{vib} + \Delta S_{rot} + \Delta S_{trans}) \approx 0.5 \text{ eV} \quad (4)$$

Therefore, we can estimate that ΔG will be exothermic only when ΔE is lower than − 0.5 eV, which is settled as a limit in Eq. 1. This condition for activity towards NRR is also found in the work of C. Ling et al. [38]. For other reactions, the analogous assessment of thermal effects is required with the corresponding change in Eq. 1.

The adsorption energies of N atoms and N_2 molecules on the HEAs microstructures were calculated as

$$\Delta E(N) = E_N - E^* - \frac{N_2^{gas-phase}}{2} \quad \text{and} \quad \Delta E(N_2) = E_{N_2} - E^* - N_2^{gas-phase} \quad (5)$$

The calculation of the first constraint used for the N adsorption, $\Delta E(Fe)$, was performed considering 2×2x5 BCC slabs on the (110) and (100) directions where results were − 1.1 eV and − 0.88 eV, respectively. $\Delta E(Ru)$ was calculated using a HCP structure in the (001) direction resulting in adsorption of − 0.78 eV. The recent work by Megha Anand et al. [37] highlights that the best NRR catalyst Ru, is followed by Fe in terms of effectiveness in catalytic activity. Instead of using the exact values of Fe and Ru adsorption energies as the constraints in Eq. 2, we set those to be − 0.7 eV and − 0.9 eV, therefore slightly shifted towards the Ru instead of Fe. If other reactions are targeted, with key rate-limiting steps in the adsorption energies, adjustments of the targeted training parameters are required and can also be chosen from other rate-limiting parameters without loss of generality.

Towards Selectivity: It is well known that most of the catalysts suffer from poor selectivity towards NRR due to the competing HER – protons being more likely to be activated and reduced on the catalytic surface than dinitrogen (N_2). Selectivity can, hence, be ranked by analyzing the averaged value of $\Delta E(H)$ and $\Delta E(N_2)$ over the microstructures of a HEA. In a first assessment, this allows the selection of the best catalysts as the ones with more positive values of $\Delta E(H) - \Delta E(N_2)$ [39]. We have tested, for 10 microstructures, if N_2 would be adsorbed exothermically once H* atoms are on the catalytic surfaces (hydrogenated surface). Unfortunately, for all cases, N_2 does not adsorb exothermically. Therefore, there is a competition between N_2* adsorption and H* adsorption and, this is mitigated if the term $\Delta E(H) - \Delta E(N_2)$ gets more positive. Moreover, the energetics of both adsorbates, H and N atoms, scale linearly (see Fig. S1 (error in the energy of hydrogen) for details, both adsorbs on a threefold site). While the relation $\Delta E(H) - \Delta E(N_2)$ might be of interest to assess absolute values of selectivity, the main concern is to *rank* the HEAs faithfully based on such parameters. To approach this, and, using the scaling relation between H and N adsorption, the energetics of the hydrogen adsorption, $\Delta E(H)$ can be exchanged by the energetics of N atoms adsorption, $\Delta E(N)$, to predict selectivity and, leading to: selectivity $= \Delta E(N) - \Delta E(N_2)$. This parameter will now be named SELE.

Potential limiting steps of the selected HEA: For the selected catalyst, a statistical approach is employed to estimate the thermodynamical barriers of the potential limiting steps.

$$N_2 + * \rightarrow N_2* \quad (6)$$

$$N_2* + (H^+ + e^-) \rightarrow NNH* \quad (7)$$

$$NH* + (H^+ + e^-) \rightarrow NHH* \quad (8)$$

The computational hydrogen electrode approach, as proposed by Nørskov [40], was applied to model the electrochemical reactions. This approach assumes a coupled electron-proton transfer simplifying the demanding calculation of solvation energies of ionic species. The free energy variation of each electrochemical/chemical reaction was calculated for 100 microstructures of the selected HEA using DFT as:

$$E_{ad} = E^*_{adsorbate} - E^* - \sum_i n_i \mu_i \quad (9)$$

where $E^*_{adsorbate}$ is the self-consistent-field (SCF) energy of the adsorbed intermediate corrected by the zero-point energy (ZPE) of the adsorbate, E^* is the SCF energy of the pure slab and n_i is the number of species i with chemical potential μ_i. Moreover, μ_H, μ_N are the chemical potentials of hydrogen and nitrogen, respectively, that are obtained as:

$$\mu_H = \frac{1}{2} E_{H_2} \quad (10)$$

$$\mu_{N_2} = E_{N_2} \quad (11)$$

$$\mu_N = \frac{E_{N_2}}{2} \quad (12)$$

$$E_{H_2,N_2} = E_{scf} + ZPE + (H_{vib} + H_{trans} + H_{rot}) - T(S_{vib} + S_{trans} + S_{rot}) + PV \quad (13)$$

The usual approach to depict the energy landscape of reaction pathways on transition metal surfaces needs to be adapted to fulfill the restriction imposed by the randomness of the HEAs. Indeed, every microstate of the structure (that together resemble the HEA surface) delivers one different energetics for the concerning reaction step. Therefore, what we can get is a distribution of energies for each associated transformation. Box plots are a common tool to report the overall patterns of a group. This summarizes important information about the group as the minimum, the first quartile, the median, the third quartile and the maximum. Here, the computed thermodynamical barriers are shown as a box plot.

3. Results

In this section, the accuracy of the developed DNN is discussed and compared to preview data reported in the literature (See *the deep neural network model* section). We also performed a deeper analysis of the relations between ALPHA, SELE, and intrinsic HEAs properties, with the resulting HEA(s) activities given in the subsection *Computed electrocatalytic activity (ALPHA)*. Finally, the most promising novel HEAs for NRR are pointed out in *The selected HEAs* section and its potentials limiting steps investigated.

The deep neural network model: The DNN employed here to estimate adsorption energies of N_2 molecules and N atoms on the surface of HEAs displayed reasonable accuracy with mean absolute errors (MAEs) of 0.09 eV and 0.20 eV, respectively (Figs. 2a and 2b). One can note that the mean absolute error of N_2 adsorption is below the typical resolution of DFT while the N adsorption shows a slightly higher error. In context to this, we would like to remind the reader that we have used the hypothesis that bond formation is a local process, and hence that the adsorption energies can be obtained by specifying elements close to adsorbates and their location. However, the model assumes symmetric adsorption sites as input parameters. This might be one of the causes of the better accuracy of the model found for N_2 adsorption than the model found for N adsorption since N_2 sits on the top site in a very symmetric environment (only one species is accounted for in region one, Fig. 2). On the other hand, N atoms sit on threefold HPC sites. Therefore, symmetry breaking would be observed depending on the coordinating species,

leading to higher errors in the built model (three species are considered in region one for this case). Still, others have reported ML predicted MAEs of about 0.2 eV regarding the DFT adsorptions energies [41], which inherently also has an error of about 0.2 eV within Beef-vdW functional [28,29]. Therefore, it pays off the employment of these models in pro of a considerable gain in computational time, allowing the removal of unpromising catalysts to be experimentally processed or by DFT calculations.

Computed electrocatalytic activity (ALPHA): ALPHA and SELE were calculated for three thousand randomly created quinary HEAs of the elements Mo, Cr, Mn, Fe, Co, Ni, Cu, and Zn. The relationship between ALPHA and SELE is displayed in Fig. 3(a) and (b). For this task, two thousand microstates of each created HEA were considered to assess the averaged quantities for SELE and the probabilities associated with ALPHA. Higher and lower values of SELE lead to lower values of ALPHA. An optimal value is obtained when SELE is between − 0.25 and 0.0, building a volcano-shaped relationship. Interestingly, the shape obtained for this relationship is also reproduced for ALPHA vs. averaged N adsorption energies. Hence, the averaged N adsorption energies emerge as the main influencing factor for SELE. The averaged N_2 adsorption appears as an almost fixed shift in SELE since they are computed as the average of cases with adsorptions higher than 0.5 eV. Hence, minimal variance is revealed when comparing distinct HEAs. As expected, the cases with higher ALPHA have averaged N adsorption energy around − 0.75 eV – the $\Delta E_N(Ru) = -0.78$ eV since ALPHA is set to maximize the probability of sites with adsorption similar to Ru.

Something interesting differentiates the case studied here from the volcano-shapes reported for NRR in the literature [23,36]. HEAs with the same averaged N adsorption (SELE) can display different activities (Fig. 2a), producing a volcano relation where data is spread *inside* the volcano shape. Two characterizing cases were selected for further analysis to gain insights into the obtained relationship. The first case, $Mo_{0.38}Fe_{0.31}Co_{0.19}Ni_{0.06}Cu_{0.06}$, has high ALPHA of 0.14 with a SELE value of − 0.15, while the second case, $Mo_{0.25}Cr_{0.06}Mn_{0.31}Cu_{0.06}Zn_{0.31}$, has ALPHA 0.00 and SELE − 0.15 eV. Though both have similar averaged N adsorption energies of − 0.75 eV and − 0.68 eV (hence, similar SELE), their distributions are completely different (Fig. 3d). Most cases end up in the required *P(N)* region for $Mo_{0.38}Fe_{0.31}Co_{0.19}Ni_{0.06}Cu_{0.06}$. For $Mo_{0.25}Cr_{0.06}Mn_{0.31}Cu_{0.06}Zn_{0.31}$, the cases are distributed on high energy and low energy values, leading to low ALPHA, yet similar SELE. The problem faced here has a multi-dimensional character, and due to the need to get averaged quantities, information is lost, thus, explaining the filled volcano-shaped relation between ALPHA vs. SELE.

Adsorption energies are widely employed to characterize activities in distinct fields of electrocatalysis [23,36,37]. Here, the direct application of the similar quantity, averaged N adsorption as the descriptor of catalytic activity of HEAs towards NRR, is shown to be insufficient to uniquely characterize each HEA, as discussed above. The plot of the averaged valence electrons in the occupied *d* orbitals (γ) vs. the averaged adsorption energies of N and N_2 brings insights into how to properly explore and develop a unique descriptor for the activity of HEAs (Fig. 4). N and N_2 adsorption strength correlate with the conventional approach to analysing the *d*-band center of transition metals [42]. This is in our view closely associated with the number of valence *d* electrons in the system and, of course, the energetic position of the states. The results displayed a close linear relation for the case of averaged N adsorption energies with R^2 of 0.76 (R^2 = goodness of the linear relation), but a widespread data point for the case of N_2 averaged adsorption energies, R^2 of 0.45. Here, calculations of N_2 adsorption on the microstructures are performed on the top site. So, the value of valence electrons in the occupied *d* orbital of the species where N_2 is adsorbed must have a much stronger influence than the averaged relation inherent in γ. Hence, γ alone cannot fully describe the averaged N_2 adsorptions. On the other hand, this issue is mitigated in the description of averaged N adsorption by the stronger influence of the three atoms coordinating the adsorbate, threefold HCP. Hence, γ results in a better descriptor for the averaged N adsorption energy. Again, information is lost when performing the averages and there exists a need to introduce a second property to better correlate the averaged adsorption and γ.

Electronegativity measures the electron affinity of certain elements

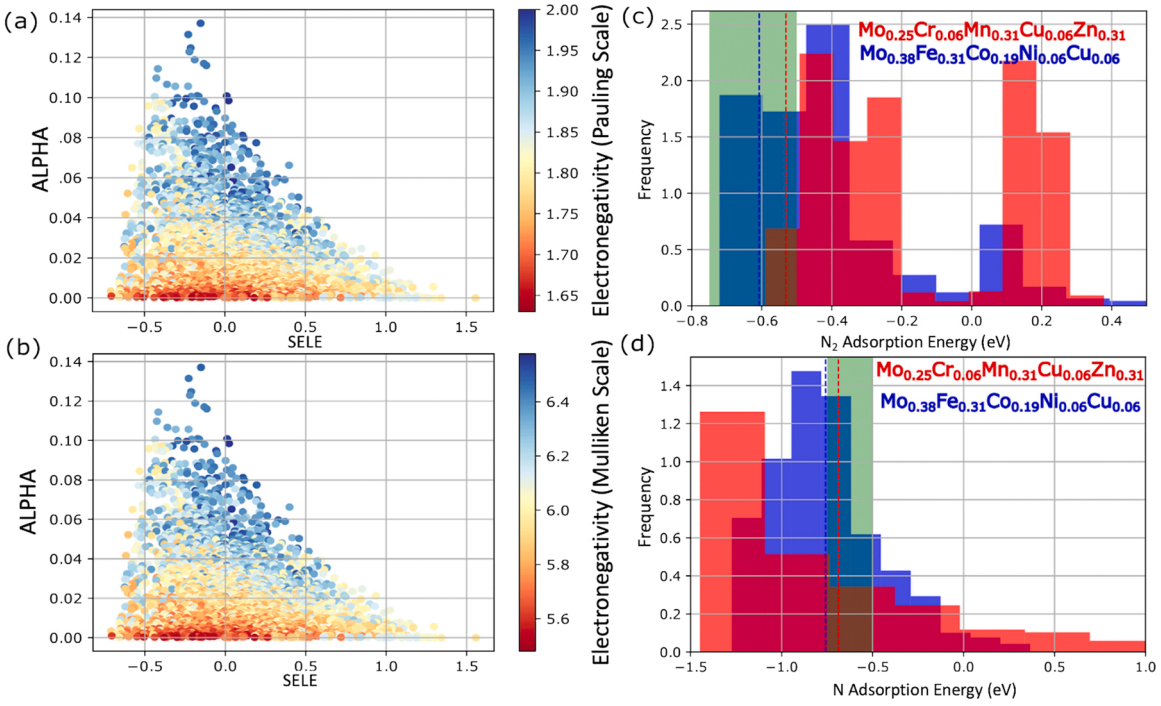

Fig. 3. Relationships between ALPHA and SELE where the color map displays the relationship between electronegativities in the (a) Pauling and (b) Mülliken scalings. (c) Histogram of N_2 adsorptions of $Mo_{0.38}Fe_{0.31}Co_{0.19}Ni_{0.06}Cu_{0.06}$ (blue) and $Mo_{0.25}Cr_{0.06}Mn_{0.31}Cu_{0.06}Zn_{0.31}$ (red). Blue and red dashed lines represent the averaged adsorption of N_2 molecules with energies higher than 0.5 eV. (d) Histogram of N adsorption of $Mo_{0.38}Fe_{0.31}Co_{0.19}Ni_{0.06}Cu_{0.06}$ (blue) and $Mo_{0.25}Cr_{0.06}Mn_{0.31}Cu_{0.06}Zn_{0.31}$ (red). Blue and red dashed lines represent the averaged adsorption of N molecules.

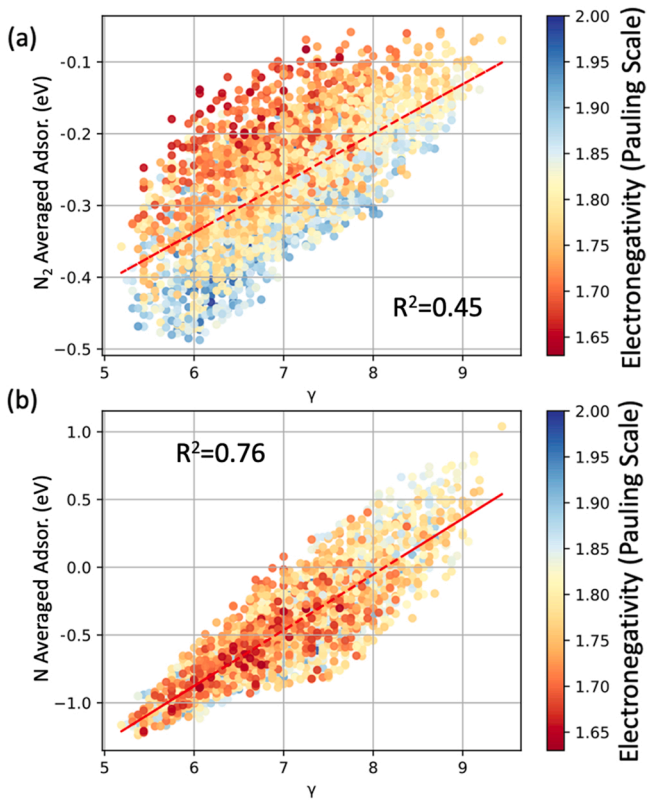

Fig. 4. : *Relationships between averaged N adsorption* vs. averaged valence electrons in the occupied *d* orbitals (γ) *(a) and averaged N_2 adsorption* vs. γ (b). The color map is added as the weighted-averaged electronegativity of the HEAs (ELE) in the Pauling scaling.

when a covalent bond is formed. Under the assumption that electronegativity would influence the redistribution of *d* electrons during the bond formation between adsorbate and catalytic surface, H. Xu et al. [43] showed that electronegativity could be employed together with the number of *d* electrons of a species as a descriptor of the O and OH adsorption energies on single metal catalysts. Using the HEA's averaged electronegativity in the plot of N_2 vs. γ as a color map, one sees that thought at same γ, *and* different averaged N_2 values are observed. Moreover, these values mainly vary with the weighted-averaged electronegativity of the HEAs (we will name the weighted averaged electronegative ELE from now on). Generally, higher ELE leads to more negative values of averaged N_2 adsorption, and inspecting the relationship between the averaged N_2 adsorption energy vs. γ/ELE (Fig. S5) a better R^2 of 0.58 is obtained in comparison to the previews value of R^2 0.45 for averaged N_2 adsorption energy vs. γ. This reflects in the volcano plot (Fig. 3a), where higher activities are found for the cases with higher ELE once the probability of finding N_2 adsorption exothermically increases under these circumstances.

As the conventional (Pauling) electronegativity scale is defined from covalent bonding, it causes concerns in metallic alloys with domination of metallic bonding. Therefore, we have also assessed how the obtained relations behave when changing the electronegativity scale (Fig. 3a-b and S6). Clearly, no change is observed when varying from the Pauling scale to the Mülliken scale defined from the arithmetic mean of the ionization energy and the electron affinity (these electronegativity measures scale linearly for the species investigated here, Fig. S7). On the other hand, no correlation between ALPHA and the electronegativity employing the Allen scale (The Allen scale is the average one-electron energy of the perceived valence shell electrons in the ground state in the free atom) is observed (Fig. S6d). Moreover, as the electronegativity could be considered a non-ideal descriptor in a metallic alloy, we explored the possibility of using the averaged work functions of the HEA as a further modification of γ as a descriptor of ALPHA where the work functions are computed for the pure bulk phases and, further, weight-averaged for the HEAs. This approach displayed no correlation with ALPHA (Fig. S6c), and together with the lack of correlation with the average one-electron energy in the Allen electronegativity, one can summarize that the local environment and effects beyond single atom properties are vital in constructing a descriptor for charge transfer in-between elements and catalytic activity of the HEAs.

The obtained relations indicate that ALPHAs of HEAs can be conveniently described by *ELE* and γ, properties easily assessed by knowing the HEAs composition and concentrations. The relation between activity (ALPHA) as a function of γ and ELE shows that higher activities are more likely to be obtained when γ is between 6 and 6.5 and ELE is higher than 1.9 (Fig. S8). It is also important to emphasize that calculations were performed here in an FCC (111) surface, and, experimentally, the HEAs phases can vary. To, somehow, capture this information, another construction for the description of the catalytic activity is constructed on the VEC of HEAs (VEC and γ scales linearly, hence, similar relation with ALPHA). Sheng Guo et al. [44] showed that HEAs with VEC higher than eight must likely form FCC structures. This similarity allows the removal of cases where the HEAs come with VEC smaller than 8, increasing the probability of getting an FCC phase upon synthesis procedure (emphasis here is given to an FCC lattice just because calculations were performed with this structure). Fig. 5 graphically shows this analysis by plotting the values of ELE vs. VEC of each HEA together with their APLHA as the color map. Higher ALPHA values are more likely to be obtained when ELE is higher than 1.9 and VEC is between 7.5 and 8.5. Hence, a map towards higher ALPHA(S) is found only using intrinsic properties of the HEAs like VEC and ELE.

4. The selected HEAs

The selected catalysts' cases presenting ALPHA higher than 0.1 are summarized in Table 1. We have grouped HEAs in two sets: *i)* the three cases with the highest ALPHA and *ii)* the cases with ALPHA higher than 0.1 and, hence, ranked based on SELE. The highest ALPHA is obtained for $Mo_{0.38}Fe_{0.31}Co_{0.19}Ni_{0.06}Cu_{0.06}$. On the other hand, C. J. H. Jacobsen et al. [45] have shown that MoCo is a promising catalyst for electrocatalytic ammonia production. Therefore, it is not surprising that $Mo_{0.38}Mn_{0.06}Fe_{0.13}Co_{0.38}Ni_{0.06}$ and $Mo_{0.31}Mn_{0.06}Fe_{0.13}Co_{0.44}Cu_{0.06}$, having balanced values between Mo and Co and minor concentrations of other species, display high activity. This also confirms the robustness of the screening strategy employed in this work.

The second set of compounds ranked based on selectivity displayed $Mo_{0.44}Co_{0.38}Ni_{0.06}Cu_{0.06}Zn_{0.06}$ as the best option. Again, the balanced

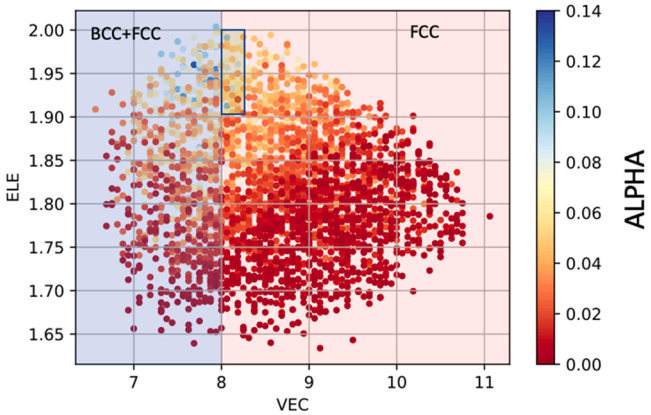

Fig. 5. Relationship between ELE vs. VEC and ALPHA as the color map. This graphic emphasizes the possibility of selecting active HEAs for ammonia production using directly assessable properties of the HEAs.

Table 1
ALPHA, SELE, VEC, ELE, δ(%), and Ω for selected HEAs. The table section with "Activity" stands for the best HEAs ranked based on ALPHA. The table section with "Selectivity" " stands for the best HEAs ranked on, ALPHA > 0.1 and the highest selectivity.

Activity						
HEA	ALPHA	SELE	VEC	ELE	δ (%)	Ω
$Mo_{0.38}Fe_{0.31}Co_{0.19}Ni_{0.06}Cu_{0.06}$	0.14	- 0.15	7.75	1.97	5.8	57.9
$Mo_{0.38}Mn_{0.06}Fe_{0.13}Co_{0.38}Ni_{0.06}$	0.12	- 0.23	7.69	1.96	5.9	5.0
$Mo_{0.31}Mn_{0.06}Fe_{0.13}Co_{0.44}Cu_{0.06}$	0.12	- 0.21	7.69	1.96	5.4	5.2
Selectivity						
HEA	ALPHA	SELE	VEC	ELE	δ(%)	Ω
$Mo_{0.44}Co_{0.38}Ni_{0.06}Cu_{0.06}Zn_{0.06}$	0.10	0.01	8.06	1.99	5.7	2.1
$Mo_{0.31}Fe_{0.31}Co_{0.25}Ni_{0.06}Cu_{0.06}$	0.12	-0.12	7.94	1.96	5.3	44.8
$Mo_{0.31}Fe_{0.38}Co_{0.19}Ni_{0.06}Cu_{0.06}$	0.12	-0.13	7.88	1.95	5.3	120.9

Mo-Co ratio leads to high activity while introducing Zn, Cu, and Ni in small quantities, leads to an increased value of SELE. Furthermore, species with higher VEC (VEC $\propto \gamma$) present lower bond strength between N atoms and the catalytic surfaces, pushing the SELE to more positive values. Interestingly, all selected cases presented ELE close to 2 since, generally, this pushes the N_2 adsorption towards more negative values, thus, resulting in higher ALPHA.

Though HEAs formed from quinary components of the elements Mo, Cr, Mn, Fe, Co, Ni, Cu, and Zn were randomly created in this work, the best HEAs serving as novel catalysts for NRR are mainly formed of Mo-Fe-Co and with minor or non-quantities of other species. Moreover, at least 30% of the HEAs are made of Mo for all cases. N_2 molecules on transition metal surfaces correlate with the *d* band center position with respect to the Fermi level of the transition metal due to the "push-pull" mechanism with σ-donation and π * -back donation [42]. Amongst the investigated species, Mo is the one with *d* band center closer to the Fermi level [46], thus, resulting in a higher probability of delivering strong N_2 adsorption. This in turn increases the value of ALPHA. Aiming to confirm this hypothesis, the adsorption energy of N_2 is calculated (see Fig. S3 for details) and displays the stronger adsorption on Mo as compared to other species. Therefore, Mo can be considered as the main N_2 molecules fixating center on the catalytic surface of the HEA during the NRR cycling. While higher amounts of Mo (yet still inside the high entropy alloy stability zone) would probably assist in the activation of N_2 molecules, but would also result in higher adsorption energies for the N atoms, scaling with the H adsorption and thus increased HER. This implies that a too strong N adsorption leads to: *i)* very slow rates of NRR reaction, *ii)* catalytic surface poisoning. To retain selectivity and not to have predominant HER reactions, the concentration of Mo has to be balanced by introducing Co and Fe species. Considerable concentrations

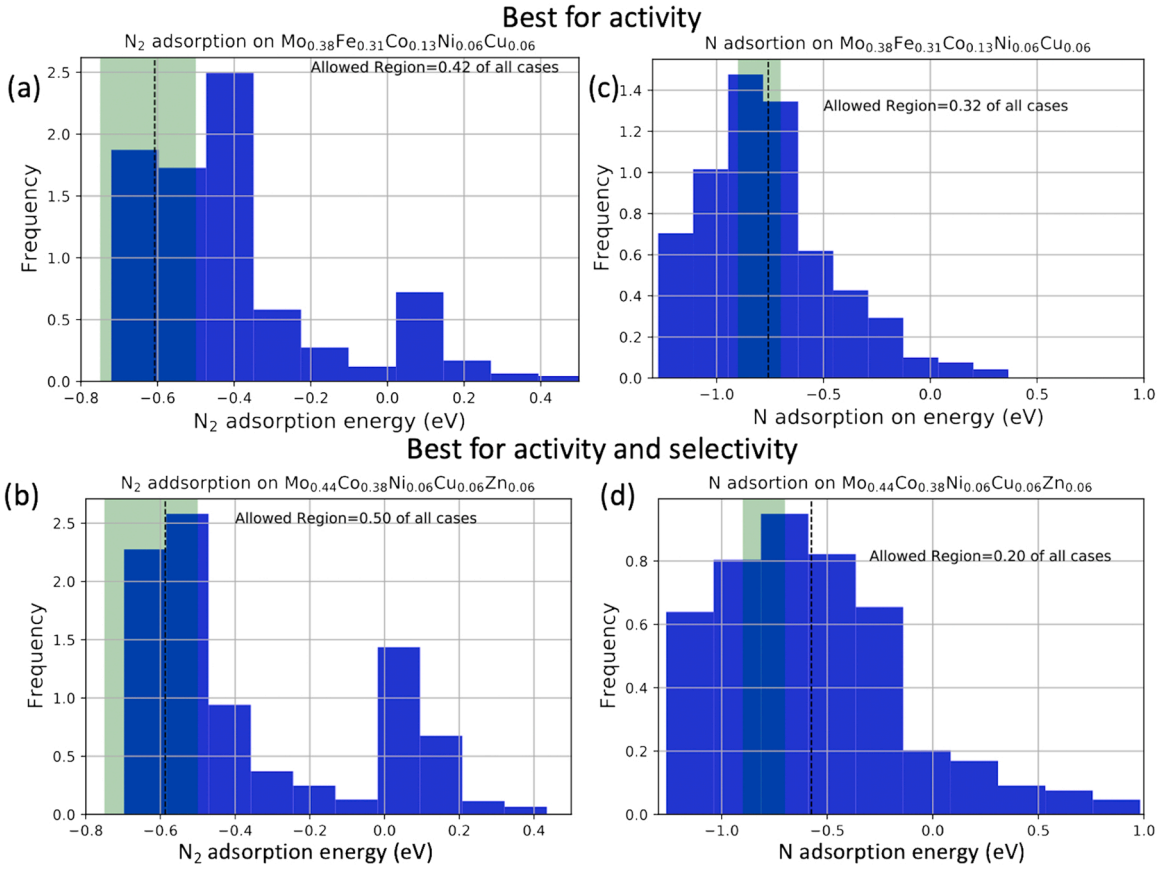

Fig. 6. Histogram of the N_2 adsorption for (a) $Mo_{0.38}Fe_{0.31}Co_{0.19}Ni_{0.06}Cu_{0.06}$ and (b) $Mo_{0.44}Co_{0.38}Ni_{0.06}Cu_{0.06}Zn_{0.06}$. Histogram of the N adsorption for (c) $Mo_{0.38}Fe_{0.31}Co_{0.19}Ni_{0.06}Cu_{0.06}$ and (d) $Mo_{0.44}Co_{0.38}Ni_{0.06}Cu_{0.06}Zn_{0.06}$.

of Cr and Mn in the HEA also deliver strong adsorption of N as compared to other species. Hence, these are not optimal options to make this balance. On the other hand, Ni, Cu, and Zn can contribute to weaker adsorption energy values.

The histograms of the HEAs $Mo_{0.38}Fe_{0.31}Co_{0.19}Ni_{0.06}Cu_{0.06}$ and $Mo_{0.44}Co_{0.38}Ni_{0.06}Cu_{0.06}Zn_{0.06}$, cases selected as the best alternatives on the two sets presented in Table 1, are displayed in Fig. 6. The relation between the probability of N_2 adsorption is directly proportional to the concentration of Mo species on the HEA, as discussed above. Here, $Mo_{0.38}Fe_{0.31}Co_{0.19}Ni_{0.06}Cu_{0.06}$ presents 42% of its active sites presenting N_2 adsorption in the exothermic region while $Mo_{0.44}Co_{0.38}Ni_{0.06}Cu_{0.06}Zn_{0.06}$ has 50% of the cases into the exothermic region (Fig. 6). The increment in the probability of finding exothermicity in the N_2 adsorption is, here, due to the increment in Mo concentration. On the other hand, the chance of finding sites with N adsorption energy close to the obtained for Ru is smaller for the case $Mo_{0.44}Co_{0.38}Ni_{0.06}Cu_{0.06}Zn_{0.06}$, 20% of the sites, in comparison to $Mo_{0.38}Fe_{0.31}Co_{0.19}Ni_{0.06}Cu_{0.06}$ presenting 32% of the sites in the optimal region. $Mo_{0.44}Co_{0.38}Ni_{0.06}Cu_{0.06}Zn_{0.06}$ exhibits sites with N adsorption energy as positive as 1 eV, and this is due to the higher concentration of species with higher VEC like Ni, Cu, and especially Zn. While this is positive to the selectivity of the HEA pushing the average N adsorption to − 0.57 eV as compared to − 0.76 eV in $Mo_{0.38}Fe_{0.31}Co_{0.19}Ni_{0.06}Cu_{0.06}$, this comes at the price of lower activity.

The tendency of a HEA to form a solid solution instead of dissociating into multiple phases can be determined via either combination of (Caloric and electrochemical) experimental measurements or theoretically via quantum mechanical calculations of alloy bonding, effects of lattice entropy from mixing, and temperature effects. X. Yang et al. [47] have demonstrated that estimations can be obtained via empirical data that estimates atomic sizes, formation enthalpy and configurational entropy. When the terms $\delta = \sqrt{\sum_{i=1}^{N} C_i\left(1-\frac{r_i}{r^{ave}}\right)^2} \leq 6.6\%$ and $\Omega = \frac{T_m \Delta S_{mix}}{|\Delta H_{mix}|} \geq 1.1$ the HEA might form a solid solution. Here, δ is a parameter gauging the atomic size difference that depends on, C_i, the atomic percentage of ith component, r_i atomic radius of ith component and r^{ave} the averaged atomic radius. Ω parameter depends on the concentration weighted averaged melting temperature, T_m, the configurational entropy $\Delta S_{mix} = -R\sum_{i=1}^{N} C_i \ln C_i$ and mixing enthalpy $\Delta H_{mix} = \sum_{i,j}^{N} C_i C_j 4H_{i,j}$ where $H_{i,j}$ is the mixing enthalpy of binary alloys computed based on Miedema macroscopic model and obtained in the work of A. Takeuchi et al. [48].

Apart from predicted activity, the individual concentrations of the elements and their respective atomic radius need to be taken into account also for the predicted HEAs. As such, it is a compromise to retain an entropically stabilized structure and, at the same time, change the composition to strive for higher activity without sacrificing too much of the entropic stabilization and thus increasing the risk of precipitation and phase separation for some of the elements. For all pointed HEAs the values of δ are smaller than 6.6%, and values of Ω are higher than 1.1 (Table 1). Hence, these HEAs would likely form a solid solution as previously described in the introduction.

We selected the best case in Table 1, $Mo_{0.38}Fe_{0.31}Co_{0.19}Ni_{0.06}Cu_{0.06}$, to perform a comparative analysis of the thermodynamical barriers of the potential limiting steps with the case of Fe(111). The energetics of the reactions for Eqs.(6–8) are displayed in box plot format for the HEA and as red lies for the case of Fe(111) (Fig. 7).

The first step, the N_2* adsorption, is endothermic on the Fe(111) surface, while for at least 25% of the 100 microstates of the HEA, this reaction becomes exothermic. Since, N_2 capturing is one of the main issues in NRR, the existence of local sites on the HEA surface with strong N_2 bonds is considered a plus for the electrochemical NRR. The activation of the N_2 * is the second investigated reaction transformation. There, in the case of Fe, the thermodynamical barriers is 1.1 eV. This means, based on the computational hydrogen electrode approach, that

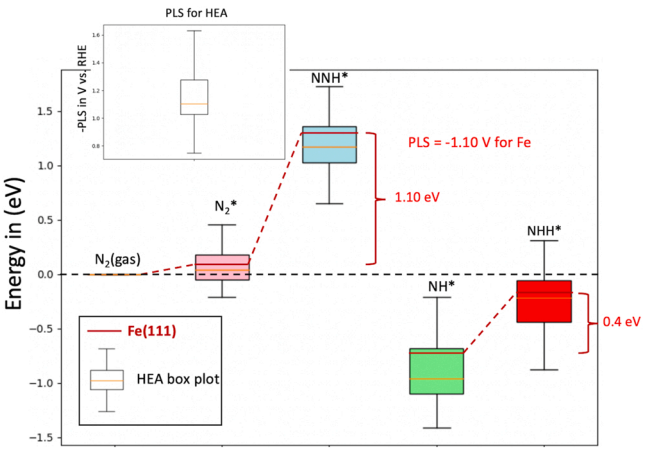

Fig. 7. Free energy diagram of the PLS of the distal NRR on the selected HEA for key intermediates along the partial reaction coordinate, and FCC Fe(111) at 0 V vs. RHE. In the inset part, one can see the box plot of the PLS for the HEA case.

at leads a potential of 1.1 V vs. RHE is needed to activate N_2* and form NNH* on iron. This picture changes for the case of the HEA. There, the lowest observed case displays a thermodynamical barrier of about 0.74 eV, while at least 25% of the 100 tested microstates of the HEA display barriers lower than 1 eV. Finally, for the desorption of the NH* and forming NH_2 * , thermodynamical barriers go from 0 eV up to 0.6 eV for the HEA vs. 0.4 eV for the case of Fe. Certainly, considering the distal pathway, the first activation of the N_2* molecule is the PLS. As demonstrated here, the randomness of the HEA surface opens up the possibility of lower PLSs as compared with the case of Fe(111) and still keeping the desorption of the NH* in a reasonable energetic value.

All the above results are expected to be directly applicable for NRR in gas-phase or in H_2O/N_2 vapor conditions as in a gas diffusion cell, while several additional considerations have to be taken into account in a practical application in a solid-liquid reaction cell. First, one needs to consider the low N_2 solubility in water (1.3×10^{-3} mol/L) [13] together with the high adsorption energies of H_2O* , OH* and H* on the catalytic surface that might create a water coverage, hydroxylation or hydrogen coverage in aqueous electrochemical cells depending on the conditions regarding electrolyte pH and the employed electrochemical potential. These points can limit the N_2 coverages on the catalytic surface, hence, deteriorating the delivered FE and activity (besides the dominant kinetics of HER over NRR [49]). In this context, even with an optimized catalyst, values of activity and FE could be way off from the expected due to the lack of available catalytic sites for the NRR reaction to proceed. One way to mitigate such issues is to work with a gas-diffusion electrode (GDE) that increases the N_2 coverage by adjusting the back N_2 pressure. In conjunction with an optimized catalyst, this strategy can facilitate the activity towards NRR due to the increased N_2 coverage and the suppressed H_2O presence that inhibit HER and surface coverages with water or hydroxyl groups, hence, increasing FE towards NH_3. Another option is the application of an aprotic electrolyte with increased N_2 solubility [50,51]. This would also promote the N_2 coverage and mitigate HER. Though HEAs concentration and compositions were optimized to deliver higher catalytic activity and selectivity towards NRR, most of the discussions presented here need to be carefully evaluated when an aqueous electrochemical cell is considered. As long as the underlying electronic properties of the HEA surface is consistently scaled to lower N_2 and N adsorption energies upon hydroxylation of the surface, the results can be directly transferrable. However, also potential decrease of the frequency of competing N_2 fixation and effects from differently induced kinks and terraces in-between different compositions would be required to behave in a scalable way compared to the flat surfaces screened here. For differences in any of these scalings, a

case-to-case investigation has to be performed for the HEAs and their corresponding hydroxylated surfaces and surface Pourbaix diagrams, to evaluate and rank the most interesting HERs.

Another point that has to be carefully evaluated is the selection of parameters used in this work to define what is an efficient HEA for NRR. Within the probabilistic approach, we selected HEAs compositions that maximize the number of sites endothermically adsorbing N_2 and also adsorbing N atoms (descriptor of catalytic activity) with adsorption energy close to Ru, as explained in the methods section. Even though this approach leads to the identification of active HEAs towards NRR, it also selects compositions with considerably high H* . This means that the selectivity can be deteriorated and also the activity due to the low coverage of N_2. Kani et al. [13] hypothesized that the most efficient catalyst for NRR, instead, would be the one with lower hydrogen adsorption H* providing lower H coverage and also lower HER activity – higher activation barrier. This option would allow the application of lower cathodic potentials without fully covering the catalytic surface with H atoms. Moreover, hydroxylation of the catalytic surface would be partially suppressed due to the destabilization of the OH groups adsorption, hence, facilitating the existence of active sites for the N_2 adsorption and lower potentials would likely lead to higher current densities. In our opinion, however, this would lead to intrinsically low NRR rates due to the increment of the thermodynamical limiting step of the NRR path. Therefore, the definition of what is a highly efficient catalyst for NRR is a gray zone that depends, amongst other things, on the experimental conditions in place and which rate one wishes to achieve. The approach presented in this work is flexible, however, and can easily be modified toward desired selectivities and rates to fit experimental conditions beyond the ones proposed in this work.

5. Concluding remarks

By employing DFT together with Machine Learning and deep neural network techniques, a screening protocol enabling a rational selection of novel catalysts for NRR was developed to search over a large compositional space of HEAs. Activities and selectivities were computed by a probabilistic approach that incorporates the adsorption of N, H, and adsorption of N_2 atoms. The computed HAE(s) activities reveal a volcano-shaped relationship with $Mo_{0.38}Fe_{0.31}Co_{0.19}Ni_{0.06}Cu_{0.06}$ located on the top of the volcano. Moreover, a rank based on selectivity and activity pointed to $Mo_{0.44}Co_{0.38}Ni_{0.06}Cu_{0.06}Zn_{0.06}$ as an alternative option that balances activity and selectivity. We also include a critical analysis of different aspects of electronegativity in connection to the work function of the elements showing that the local composition and charge transfer are necessary to formulate key descriptors of catalytic activity. Instead, valence electron concentration of HEAs with either different energy *d*-states or electronegativity, forms descriptors of the catalytic activity. The approach shows a promising pathway to conveniently screen candidates for catalytic activity and selectivity for a given catalytic reaction, here exemplified by the NRR reaction. The screening disclosed and quantified existing relationships between HEAs composition and catalytic activities towards NRR that bears the promise of accelerating the search for complex NRR catalysts.

Declaration of Competing Interest

The authors declare that they have no known competing financial interests or personal relationships that could have appeared to influence the work reported in this paper.

Data Availability

Data will be made available on request.

Acknowledgments

This work was financially supported by the European Union's Horizon 2020 research and innovation programme under the call H2020-LC-SC3-2020-RES-RIA in the TELEGRAM project [grant agreement No 101006941]. The computations were enabled by resources provided by the Swedish National Infrastructure for Computing (SNIC) via the project SNIC 2021/5-282, and funding by the Swedish Research Council through grant agreement no. 2019-05591.

Additional Information

Supplementary information is available in the online version.

Appendix A. Supporting information

Supplementary data associated with this article can be found in the online version at doi:10.1016/j.nanoen.2022.108027.

References

[1] U.S.E.I. Administration Energy Inf. Adm What Is. Energy? 2017.
[2] S. Giddey, S.P.S. Badwal, A. Kulkarni, Review of electrochemical ammonia production technologies and materials, Int. J. Hydrog. Energy 38 (2013) 14576–14594, https://doi.org/10.1016/j.ijhydene.2013.09.054.
[3] J.W. Yeh, S.K. Chen, S.J. Lin, J.Y. Gan, T.S. Chin, T.T. Shun, C.H. Tsau, S.Y. Chang, Nanostructured high-entropy alloys with multiple principal elements: novel alloy design concepts and outcomes, Adv. Eng. Mater. 6 (2004) 299–303, https://doi.org/10.1002/adem.200300567.
[4] B. Cantor, I.T.H. Chang, P. Knight, A.J.B. Vincent, Microstructural development in equiatomic multicomponent alloys, Mater. Sci. Eng. A 375–377 (2004) 213–218, https://doi.org/10.1016/j.msea.2003.10.257.
[5] A. Amiri, R. Shahbazian-Yassar, Recent progress of high-entropy materials for energy storage and conversion, J. Mater. Chem. A 9 (2021) 782–823, https://doi.org/10.1039/d0ta09578h.
[6] Y. Sun, S. Dai, High-entropy materials for catalysis: a new frontier, Sci. Adv. 7 (2021) 1–24, https://doi.org/10.1126/sciadv.abg1600.
[7] M. Fu, X. Ma, K. Zhao, X. Li, D. Su, High-entropy materials for energy-related applications, IScience 24 (2021) 102177, https://doi.org/10.1016/j.isci.2021.102177.
[8] J.K. Pedersen, T.A.A. Batchelor, D. Yan, L.E.J. Skjegstad, J. Rossmeisl, Surface electrocatalysis on high-entropy alloys, Curr. Opin. Electrochem. 26 (2021), 100651, https://doi.org/10.1016/j.coelec.2020.100651.
[9] N. Cao, G. Zheng, Aqueous electrocatalytic N2 reduction under ambient conditions, Nano Res 11 (2018) 2992–3008, https://doi.org/10.1007/s12274-018-1987-y.
[10] C. Yang, Y. Zhu, J. Liu, Y. Qin, H. Wang, H. Liu, Y. Chen, Z. Zhang, W. Hu, Defect engineering for electrochemical nitrogen reduction reaction to ammonia, Nano Energy 77 (2020), 105126, https://doi.org/10.1016/j.nanoen.2020.105126.
[11] N. Furuya, H. Yoshiba, Electroreduction of nitrogen to ammonia on gas-diffusion electrodes loaded with inorganic catalyst, J. Electroanal. Chem. 291 (1990) 269–272, https://doi.org/10.1016/0022-0728(90)87195-P.
[12] Y. Ren, C. Yu, X. Tan, H. Huang, Q. Wei, J. Qiu, Strategies to suppress hydrogen evolution for highly selective electrocatalytic nitrogen reduction: challenges and perspectives, Energy Environ. Sci. 14 (2021) 1176–1193, https://doi.org/10.1039/d0ee03596c.
[13] N.C. Kani, A. Prajapati, B.A. Collins, J.D. Goodpaster, M.R. Singh, Competing effects of pH, cation identity, H_2O saturation, and N_2 concentration on the activity and selectivity of electrochemical reduction of N_2 to NH_3 on electrodeposited Cu at ambient conditions, ACS Catal. 10 (2020) 14592–14603, https://doi.org/10.1021/acscatal.0c04864.
[14] Y.C. Hao, Y. Guo, L.W. Chen, M. Shu, X.Y. Wang, T.A. Bu, W.Y. Gao, N. Zhang, X. Su, X. Feng, J.W. Zhou, B. Wang, C.W. Hu, A.X. Yin, R. Si, Y.W. Zhang, C.H. Yan, Promoting nitrogen electroreduction to ammonia with bismuth nanocrystals and potassium cations in water, Nat. Catal. 2 (2019) 448–456, https://doi.org/10.1038/s41929-019-0241-7.
[15] D. Zhang, H. Zhao, X. Wu, Y. Deng, Z. Wang, Y. Han, H. Li, Y. Shi, X. Chen, S. Li, J. Lai, B. Huang, L. Wang, Multi-site electrocatalysts boost pH-universal nitrogen reduction by high-entropy alloys, Adv. Funct. Mater. 31 (2021) 1–8, https://doi.org/10.1002/adfm.202006939.
[16] T.A.A. Batchelor, J.K. Pedersen, S.H. Winther, I.E. Castelli, K.W. Jacobsen, J. Rossmeisl, High-entropy alloys as a discovery platform for electrocatalysis, Joule 3 (2019).
[17] J.K. Pedersen, T.A.A. Batchelor, A. Bagger, J. Rossmeisl, High-entropy alloys as catalysts for the CO_2 and CO reduction reactions: experimental realization, ACS Catal. 10 (2020) 3658–3663, https://doi.org/10.1021/acscatal.9b04302.
[18] W.A. Saidi, W. Shadid, G. Veser, Optimization of high-entropy alloy catalyst for ammonia decomposition and ammonia synthesis, J. Phys. Chem. Lett. 12 (2021) 5185–5192, https://doi.org/10.1021/acs.jpclett.1c01242.

[19] A.R. Singh, B.A. Rohr, M.J. Statt, J.A. Schwalbe, M. Cargnello, J.K. Nørskov, Strategies toward selective electrochemical ammonia synthesis, ACS Catal. 9 (2019) 8316–8324, https://doi.org/10.1021/acscatal.9b02245.

[20] E. Tayyebi, Y. Abghoui, E. Skúlason, Elucidating the mechanism of electrochemical N_2 reduction at the Ru(0001) electrode, ACS Catal. 9 (2019) 11137–11145, https://doi.org/10.1021/acscatal.9b03903.

[21] X. Cui, C. Tang, Q. Zhang, A review of electrocatalytic reduction of dinitrogen to ammonia under ambient conditions, Adv. Energy Mater. 8 (2018) 1–25, https://doi.org/10.1002/aenm.201800369.

[22] J.K. Pedersen, T.A.A. Batchelor, D. Yan, L.E.J. Skjegstad, J. Rossmeisl, Surface electrocatalysis on high-entropy alloys, Curr. Opin. Electrochem 26 (2021) 100651, https://doi.org/10.1016/j.coelec.2020.100651.

[23] J.H. Montoya, C. Tsai, A. Vojvodic, J.K. Nørskov, The challenge of electrochemical ammonia synthesis: A new perspective on the role of nitrogen scaling relations, ChemSusChem 8 (2015) 2180–2186, https://doi.org/10.1002/cssc.201500322.

[24] Á.B. Höskuldsson, E. Tayyebi, E. Skúlason, Computational examination of the kinetics of electrochemical nitrogen reduction and hydrogen evolution on a tungsten electrode, J. Catal. 404 (2021) 362–370, https://doi.org/10.1016/j.jcat.2021.10.017.

[25] S.M. Sharada, T. Bligaard, A.C. Luntz, G.-J. Kroes, J.K. Nørskov, SBH10: a benchmark database of barrier heights on transition metal surfaces, J. Phys. Chem. C 121 (2017) 19807–19815, https://doi.org/10.1021/ACS.JPCC.7B05677.

[26] G. Kresse, J. Furthmůller, Efficient iterative schemes for ab initio total-energy calculations using a plane-wave basis set, Phys. Rev. B. 54 (1996) 11169–11186, https://doi.org/10.1103/PhysRevB.54.11169.

[27] G. Kresse, D. Joubert, From ultrasoft pseudopotentials to the projector augmented-wave method, Phys. Rev. B 59 (1999) 1758–1775, https://doi.org/10.1103/PhysRevB.59.1758.

[28] J. Wellendorff, K.T. Lundgaard, A. Møgelhøj, V. Petzold, D.D. Landis, J.K. Nørskov, T. Bligaard, K.W. Jacobsen, Density functionals for surface science: Exchange-correlation model development with Bayesian error estimation, Phys. Rev. B - Condens. Matter Mater. Phys. 85 (2012) 32–34, https://doi.org/10.1103/PhysRevB.85.235149.

[29] S. Mallikarjun Sharada, R.K.B. Karlsson, Y. Maimaiti, J. Voss, T. Bligaard, Adsorption on transition metal surfaces: Transferability and accuracy of DFT using the ADS41 dataset, Phys. Rev. B 100 (2019) 035439, https://doi.org/10.1103/PhysRevB.100.035439.

[30] J. Wellendorff, T.L. Silbaugh, D. Garcia-Pintos, J.K. Nørskov, T. Bligaard, F. Studt, C.T. Campbell, A benchmark database for adsorption bond energies to transition metal surfaces and comparison to selected DFT functionals, Surf. Sci. 640 (2015) 36–44, https://doi.org/10.1016/j.susc.2015.03.023.

[31] C.M. Clausen, J.K. Pedersen, T.A.A. Batchelor, J. Rossmeisl, Lattice distortion releasing local surface strain on high-entropy alloys, Nano Res. (2021) 035439/1–035439/13, https://doi.org/10.1007/s12274-021-3544-3.

[32] F. Chollet, Others, Keras, (2015). ⟨https://github.com/fchollet/keras⟩.

[33] Z. Geng, Y. Liu, X. Kong, P. Li, K. Li, Z. Liu, J. Du, M. Shu, R. Si, J. Zeng, Achieving a record-high yield rate of 120.9 μg NH_3 mgcat.$^{-1}$h^{-1} for N_2 electrochemical reduction over Ru single-atom catalysts, Adv. Mater. 30 (2018) 2–7, https://doi.org/10.1002/adma.201803498.

[34] D. Wang, L.M. Azofra, M. Harb, L. Cavallo, X. Zhang, B.H.R. Suryanto, D. R. MacFarlane, Energy-efficient nitrogen reduction to ammonia at low overpotential in aqueous electrolyte under ambient conditions, ChemSusChem 11 (2018) 3416–3422, https://doi.org/10.1002/cssc.201801632.

[35] Y. Yao, H. Wang, X.Z. Yuan, H. Li, M. Shao, Electrochemical nitrogen reduction reaction on ruthenium, ACS Energy Lett. 4 (2019) 1336–1341, https://doi.org/10.1021/acsenergylett.9b00699.

[36] E. Skúlason, T. Bligaard, S. Gudmundsdóttir, F. Studt, J. Rossmeisl, F. Abild-Pedersen, T. Vegge, H. Jónsson, J.K. Nørskov, A theoretical evaluation of possible transition metal electro-catalysts for N_2 reduction, Phys. Chem. Chem. Phys. 14 (2012) 1235–1245, https://doi.org/10.1039/c1cp22271f.

[37] M. Anand, B. Rohr, M.J. Statt, J.K. Nørskov, Scaling relationships and volcano plots in homogeneous catalysis, J. Phys. Chem. Lett. 11 (2020) 8518–8526, https://doi.org/10.1021/acs.jpclett.0c01991.

[38] C. Ling, Y. Ouyang, Q. Li, X. Bai, X. Mao, A. Du, J. Wang, A general two-step strategy–based high-throughput screening of single atom catalysts for nitrogen fixation, Small Methods 3 (2019) 1–8, https://doi.org/10.1002/smtd.201800376.

[39] Y. Xiao, C. Shen, T. Long, Theoretical establishment and screening of an efficient catalyst for n2electroreduction on two-dimensional transition-metal borides (MBenes, Chem. Mater. 33 (2021) 4023–4034, https://doi.org/10.1021/acs.chemmater.1c00424.

[40] J.K. Nørskov, J. Rossmeisl, A. Logadottir, L. Lindqvist, J.R. Kitchin, T. Bligaard, H. Jónsson, Origin of the overpotential for oxygen reduction at a fuel-cell cathode, J. Phys. Chem. B 108 (2004) 17886–17892, https://doi.org/10.1021/jp047349j.

[41] S. Back, J. Yoon, N. Tian, W. Zhong, K. Tran, Z.W. Ulissi, Convolutional neural network of atomic surface structures to predict binding energies for high-throughput screening of catalysts, J. Phys. Chem. Lett. 10 (2019) 4401–4408, https://doi.org/10.1021/acs.jpclett.9b01428.

[42] L.G.M. Pettersson, A. Nilsson, A molecular perspective on the d-band model: Synergy between experiment and theory, Top. Catal. 57 (2014) 2–13, https://doi.org/10.1007/s11244-013-0157-4.

[43] H. Xu, D. Cheng, D. Cao, X.C. Zeng, A universal principle for a rational design of single-atom electrocatalysts, Nat. Catal. 1 (2018) 339–348, https://doi.org/10.1038/s41929-018-0063-z.

[44] S. Guo, C. Ng, J. Lu, C.T. Liu, Effect of valence electron concentration on stability of fcc or bcc phase in high entropy alloys, J. Appl. Phys. 109 (2011) 103505/1–103505/5, https://doi.org/10.1063/1.3587228.

[45] C.J.H. Jacobsen, S. Dahl, B.G.S. Clausen, S. Bahn, A. Logadottir, J.K. Nørskov, Catalyst design by interpolation in the periodic table: Bimetallic ammonia synthesis catalysts, J. Am. Chem. Soc. 123 (2001) 8404–8405, https://doi.org/10.1021/ja010963d.

[46] A. Vojvodic, J.K. Nørskov, F. Abild-Pedersen, Electronic structure effects in transition metal surface chemistry, Top. Catal. 57 (2014) 25–32, https://doi.org/10.1007/s11244-013-0159-2.

[47] X. Yang, Y. Zhang, Prediction of high-entropy stabilized solid-solution in multi-component alloys, Mater. Chem. Phys. 132 (2012) 233–238, https://doi.org/10.1016/j.matchemphys.2011.11.021.

[48] A. Takeuchi, A. Inoue, Classification of bulk metallic glasses by atomic size difference, heat of mixing and period of constituent elements and its application to characterization of the main alloying element, Mater. Trans. 46 (2005) 2817–2829.

[49] G. Rostamikia, S. Maheshwari, M.J. Janik, Elementary kinetics of nitrogen electroreduction to ammonia on late transition metals, Catal. Sci. Technol. 9 (2019) 174–181, https://doi.org/10.1039/c8cy01845f.

[50] B.H.R. Suryanto, C.S.M. Kang, D. Wang, C. Xiao, F. Zhou, L.M. Azofra, L. Cavallo, X. Zhang, D.R. Macfarlane, Rational electrode-electrolyte design for efficient ammonia electrosynthesis under ambient conditions, ACS Energy Lett. 3 (2018) 1219–1224, https://doi.org/10.1021/acsenergylett.8b00487.

[51] F. Zhou, L.M. Azofra, M. Ali, M. Kar, A.N. Simonov, C. McDonnell-Worth, C. Sun, X. Zhang, D.R. Macfarlane, Electro-synthesis of ammonia from nitrogen at ambient temperature and pressure in ionic liquids, Energy Environ. Sci. 10 (2017) 2516–2520, https://doi.org/10.1039/c7ee02716h.

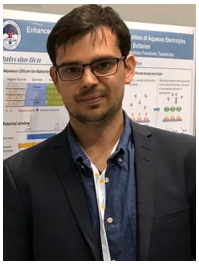

Rafael B. Araujo received his Ph.D. in Computational Physics from Uppsala University, Sweden in 2017. He worked as a postdoctoral researcher at Chalmers University of Technology and Stockholm University, Sweden. He has been continuing as a postdoctoral researcher in the group of Prof. Tomas Edvinsson at the Department of Materials Science and Engineering, Uppsala University, since September 2021. His research interests include applying a broad range of computational tools to intriguing scientific problems related to catalysis, batteries, materials for energy storage and fundamental aspects and applications of novel 2D materials.

Ilknur Bayrak Pehlivan is a senior researcher at the Department of Materials Science and Engineering, Uppsala University, Sweden. She received her Ph.D in 2013 at Uppsala University with a study on the functionalization of polymer electrolytes for electrochromic windows. Her research interest is in electrocatalyst development for integrated solar water splitting, electrochemical ammonia synthesis, direct ammonia fuel cell and electrochromic systems.

Tomas Edvinsson is professor in Solid State Physics at the Department of Materials Science and Engineering, Uppsala University, Sweden. He received his Ph.D. 2002 at Uppsala University, performed post-doctoral work at the Royal Institute of Technology, Stockholm, and research for BASF AG until 2007. He is the project leader for several national projects from the Swedish research council, the Swedish Energy Agency, and acts as reviewer for several national and international grant organizations. His research focus on fundamental investigations of low dimensional materials and their utilization in sustainable energy applications.